Germanene nanomeshes: Cooperative effects of degenerate perturbation and uniaxial strain on tuning bandgap*

Yan Su(苏燕) and Xinyu Fan(范新宇)†

Department of Physics, University of Ji'nan, Ji'nan 250022, *China*

(Received 27 May 2017; revised manuscript received 30 June 2017; published online 10 September 2017)

Based on the detailed first-principles calculations, we have carefully investigated the defect induced band splitting and its combination with Dirac cone move in bandgap opening. The uniaxial strain can split the π-like bands into π_a and π_z bands with energy interval E_{strain} to shift the Dirac cone. Also, the inversion symmetry preserved antidot can split π_a (π_z) into π_{a1} and π_{a2} (π_{z1} and π_{z2}) bands with energy interval E_{defect} to open bandgap in the nanomesh with Γ as four-fold degenerate Dirac point according to the band-folding analysis. Though the E_{defect} would keep almost unaffected, the E_{strain} would be increased by enhancing the uniaxial strain to continuously tune the gap width. Then the bandgap can be reversibly switched on/off. Our studies of the inversion symmetry preserved nanomesh show distinct difference in bandgap opening mechanism as compared to the one by breaking the sublattice equivalence in the $(GaAs)_6$ nanoflake patterned nanomesh. Here, the π-band gap remains almost unchanged against strain enhancing.

Keywords: first-principles calculation, novel two-dimensional nanostructure, bandgap engineering

PACS: 81.05.Zx, 81.05.Rm, 81.05.ue **DOI:** 10.1088/1674-1056/26/10/108101

1. Introduction

Since the successful synthesis of graphene, this marvelous material has attracted extraordinary research attention in science and technology due to its novel physical and chemical properties, which has also driven a new research field in exploring two-dimensional (2D) materials.[1–35] Owing to similar physical and chemical properties, the same column elements of carbon have also gained much attention in exploring 2D crystal structures.[12–35] Due to the fact that silicon and germanium have the same number of valence electrons as that of carbon and could have similar sp hybridization configurations, lots of efforts have been devoted on the fabrications of silicene and germanene and the investigations of their peculiar properties. Unlike their cousin element carbon, the ideal one atomic layer sheet of hexagonally arranged Si or Ge is unstable, which however would be slightly buckled.[16,17] One of them is vertically displaced of about half angstrom with respect to the other. The crucial role of buckling in germanene has been studied in detail by Nijamudheen *et al.*[17] Interestingly, it is that both silicene and germanene possess similar electronic properties as those of graphene, such as the massless fermions due to the linear dispersion relation around Dirac point and the quantum Hall effect, etc. Besides of the tremendous studies on silicene, the germanene has recently gained intensive research interest,[17–34] which could also be incorporated into nanoelectronics based on the current silicon and germanium based semiconductor industrial techniques. By depositing germanium on metal substrates, the germanene has been successfully fabricated in experiment. The (111) oriented metal surfaces are usually used as substrates, for example the germanene growth on the noble metals. Very recently, the germanene sheet was successfully fabricated on Pt (111) by Li *et al.*[19] By using Au (111) as substrate, Dávila *et al.* have also successfully grown atomically thin germanene layer.[20] Surprisingly, a very interesting recent study shows the possibilities in synthesizing germanene sheet on simple metal.[21] The Al (111) was found to be a good material to support germanene, which would surely benefit its usage in electronic devices for the low application cost compared to the ones supported on Au or Pt. The progress of germanene fabrication has paved the path for exploring its unique physical and chemical properties.

Although the synthesis of free-standing germanene monolayer has not yet been achieved, the corresponding studies on monolayer have in fact already attracted much attention on theory,[22–34] which would in turn benefit further experimental investigations. Though the massless high velocity fermions show much peculiar properties for potential applications, the band closure in germanene would however harm its usage in transistors of photoelectronics which in fact requires a practical on/off ratio. Therefore, the bandgap opening has recruited research attention as an important issue in germanene studies. The electric field,[25,26] functionalization such as hydrogenation, etc.,[27,28] and surface adsorption[29–31] have been verified to be effective for the opening bandgap in ger-

*Project supported by the National Natural Science Foundation of China (Grant Nos. 11374128 and 11674129) and partially supported by the Science and Technology Program of University of Jinan (Grant No. XKY1705).

†Corresponding author. E-mail: xyfan_ujn@163.com

© 2017 Chinese Physical Society and IOP Publishing Ltd

manene. As a contribution to the studies of germanene-based nanostructures, we have carried out detailed studies on the bandgap opening in germanene nanomeshes by employing density functional theory calculations. For a kind of nanomeshes, the Dirac cone would be folded to Γ point according to the band-folding analysis, resulting in the four-fold degenerated band crossing point at Γ. Considering in the fact of the spin degeneracy of the corresponding electrons, this point could be regarded as eight-fold degenerate point. In this paper, we actually just concentrate on studying the degeneracy in band states which could hold both the spin-up and spin-down electrons in each band. Therefore, we would like to refer this band crossing point as four-fold degenerate point, which would not affect our conclusion of the band gap opening in germanene nanomesh. By introducing a D_{6h} defect in the repeated unit cell, a sizable bandgap would be opened through the four-fold degeneracy perturbation mechanism though the inversion symmetry still remains. In this paper, the four-fold degeneracy perturbation mechanism and the strain effects are also first time combined together to tune electronic properties of germanene nanomesh, suggesting an interesting methodology for reversibly switching on/off bandgap. Furthermore, the gap width could be tuned by controlling the defect density to show attractive application potentials.

2. Computational details

We carried out detailed first-principles studies based on the density functional theory (DFT) as implemented in the Vienna *ab initio* simulation package (VASP).[36] The electron–ion and electron–electron exchange correlation interactions were calculated respectively by using the projector augmented wave (PAW) method[37] and the generalized gradient approximation (GGA) in the formalism of Perdew, Burke, and Ernzehof (PBE).[38] The solution of Kohn–Sham (KS) equation was solved by an efficient matrix diagonalization technique based on a sequential band-by-band residual minimization method.[36] The planewave basis set was adopted. The corresponding cutoff energies are 173, 208, and 250 eV for dealing with the pristine germanene sheet, the antidot patterned germanene nanomesh, and the nanomesh patterned by regularly arranging $(GaAs)_6$ nanopatches, respectively. Because the lattice constant of 5.65 Å of GaAs bulk agrees well with the 5.66 Å of germanium bulk, the $(GaAs)_6$ flake was adopt to reduce the structural distortion after substitution doping. The germanene was placed in the XY plane of the supercell which was separated by about 15 Å vacumm in Z direction to eliminate the interaction with its neighboring images. The structures were fully relaxed until the components of the Hellmann–Feynman forces acting on each atom are smaller than 0.01 eV/Å. The Monkhorst–Pack technique[38] was adopted to sample k-points in the Brillouin zone for integrating the electronic properties. For the studying of germanene with the primitive unit cell and the smallest rectangle unit, the electronic structures were calculated by using a $21\times21\times1$ k-mesh. The structural parameters of the primitive unit cell of pristine germanene were firstly optimized, which were then used to construct nanomesh. In Fig. 1, we show the schematic structure of germanene. The in plane lattices of the hexagonal primitive unit cell were calculated to be 4.06 Å and the displacement height between the sublattices of the low-buckled structure was found to be 0.69 Å, which are in good agreement with the previous data.[21] For studying the germanene nanomeshes with the large size supercells of 21.1 Å$\times$12.2 Å$\times$16 Å and 42.2 Å$\times$24.4 Å$\times$16 Å, the k-meshes of $5\times7\times1$ and $3\times5\times1$ were adopted, respectively.

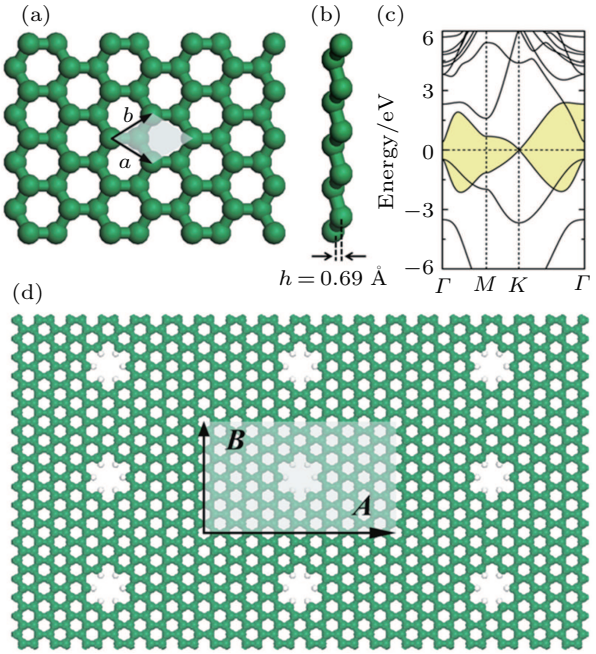


Fig. 1. (color online) The top (a) and side views (b) of the geometrical structure of germanene, and the bandstructure calculated by using the primitive unit cell (c). An anitdot-patterned orthogonal nanomesh defined by $\boldsymbol{A}\times\boldsymbol{B}$ unit is schematically illustrated in panel (d). The antidot hole edge is passivated by hydrogen.

3. Results and discussion

3.1. Bandgap opening induced by antidot

As illustrated in Fig. 1(d), an orthogonal germanene nanomesh with $\boldsymbol{A}\times\boldsymbol{B}$ unit could be patterned out by regularly arranging antidots. In experiment, the nanotechniques of block copolymer lithography, nanoparticles local catalytic hydrogenation, nanosphere lithography, and nanoimprint lithography, etc. could be used to fabricate hexagonal and orthogonal nanomeshes.[40] With the purpose to facilitate discussing the effects of uniaxal strains respectively applied along armchair and zigzag directions, we would like to concentrate on studying the orthogonal nanomeshes in this paper, whose con-

clusions could shed light on the hexagonal nanomeshes. For the isolated free-standing germanene sheet, the bandstructure calculated by using the primitive unit cell has been presented in Fig. 1(c), which has Dirac cones at K-type points. The smallest rectangle unit cell of germanene could be defined by the $\boldsymbol{A}_1 = \boldsymbol{a} + \boldsymbol{b}$ and $\boldsymbol{B}_1 = -\boldsymbol{a} + \boldsymbol{b}$ as shown in Fig. 2(a) ($\boldsymbol{a}$ and $\boldsymbol{b}$ are the basis lattices of the primitive unit cell). In comparison with the germanene studied with the primitive unit cell, we would like to hereafter refer the pristine germanene studied with the supercell $\boldsymbol{A} \times \boldsymbol{B}$ as pseudo germanene superlattice (PGS). If a perturbation such as an antidot was introduced in the periodic unit $\boldsymbol{A} \times \boldsymbol{B}$, the PGS would turn to be a real superlattice. In order to facilitate discussion, we would like to use the notation (P, Q) to account for the lattice $\boldsymbol{A} \times \boldsymbol{B}$ with $\boldsymbol{A} = P\boldsymbol{A}_1$ and $\boldsymbol{B} = Q\boldsymbol{B}_1$. Therefore, the $(1,1)$ stands for the smallest rectangle PGS $\boldsymbol{A}_1 \times \boldsymbol{B}_1$. In Fig. 2(b), we present the corresponding Brillouin zones for the primitive unit cell (the hexagonal one, h-BZ) and the $(1,1)$ PGS (the rectangle one, r-BZ). According to the band-folding analysis, the K point in the h-BZ of primitive unit cell is now folded to the T_1 ($\frac{2}{3}\boldsymbol{\Gamma}_1\boldsymbol{Y}_1$) point in the r-BZ of $(1,1)$ PGS. The corresponding bandstructure shown in Fig. 2(c) confirms the band-folding of Dirac cone to the T_1 point. Also, the $(1,3)$ PGS as schematically

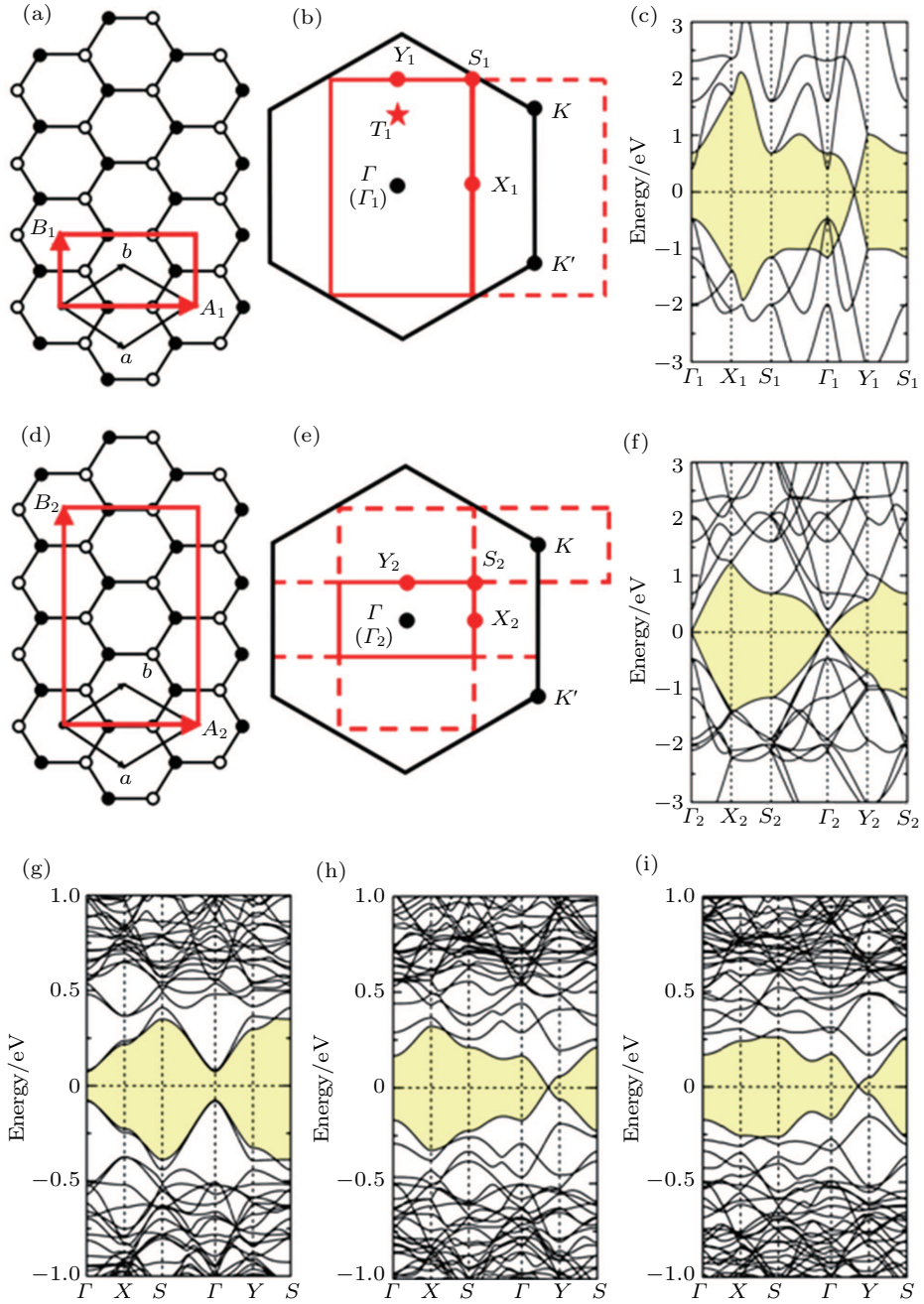


Fig. 2. (color online) The schematic structure, Brillouin zone r-BZ, and band structure for the $(1,1)$ PGS are shown in panels (a), (b), and (c), respectively. Those for the $(1,3)$ PGS are presented in panels (d), (e), and (f), respectively. The Brillouin zone h-BZ corresponding to the primitive unit cell is also shown in panels (b) and (e) for comparison. The panels (g), (h), and (i) are the band structures of the antidot-patterned $(5,6)$, $(5,7)$, and $(5,8)$ germanene nanomeshes.

shown in Fig. 2(d) has been carefully studied, whose r-BZ is shown in Fig. 2(e). Interestingly, according to the band-folding analysis, the Dirac cone is now folded to the Γ point, which could be also seen in the calculated bandstructure (see Fig. 2(f)). Based on our band-folding analysis, we found that the Dirac cone would be always folded onto the axis of the corresponding r-BZ of (P,Q) PGS no matter what value of P. However, the value of Q indeed could make difference to clarify PGSes into two categories: (i) the lattices of $Q = 3m$ (m is integer) with Dirac point being folded to Γ to form four-fold degeneracy; and (ii) the other ones with the T-type point $(\frac{2}{3}\boldsymbol{\Gamma Y})$ as the two-fold degenerate Dirac point. Introducing a defect into the repeated unit of PGS would make real superlattice due to the modulation of Born–von Karman boundary conditions.[41,42] To shed light on the experimentally synthesized nanomesh with circular vacancy hole, we would like to concentrate on studying the hexagonal antidot patterned germanene nanomesh, in which the inversion symmetry remains. Interestingly, the D_{6h} antidot acts quite differently on bandgap opening of germanene nanomeshes. In Figs. 2(g)–2(i), the Ge_6 antidot patterned $(5,6)$, $(5,7)$, and $(5,8)$ nanomeshes are studied for illustration (In order to facilitate discussion, we would like to use the notation Ge_n to account for the antidot formed by removing a n-atom D_{6h} germanium nanoflake from the germanene with the hole edge passivated by hydrogen). After introducing antidots, we have estimated their structural stabilities by using the first-principles molecular dynamics simulations (MD), which last for 10 ps with the time step of 1 fs. During the MD simulations, the $(5,6)$, $(5,7)$, and $(5,8)$ superlattices could withstand against structural collapse, suggesting good stabilities. The $(5,6)$ superlattice, which should have band closing Dirac point at Γ, has been opened a sizeable bandgap. However, the antdot does not affect the semimetal nature of the $(5,7)$ and $(5,8)$ nanomeshes. To conclude, the perturbation attributed to the inversion symmetry preserved defect can lift the four-fold degeneracy at Γ point to open a sizable bandgap in (P,Q) nanomesh with $Q = 3m$, while it cannot for the other studied nanomeshes, suggesting a different mechanism as compared to the one by breaking the sublattice equivalence. Here, we would like also to mention the effects of the magnetic coupling. Providing to remove the hydrogen atoms on the antidot hole edge, the resulted magnetism distribution would affect the electronic properties. The antiferromagnetic coupling configuration would break the sublattice equivalence to open bandgap in all the types of germanene nanomeshes. However, the ferromagnetic coupling configuration still holds the inversion symmetry. The presence of antidot would then only open bandgap in the superalttice (P,Q) with $Q = 3m$.

3.2. Dirac cone move and splitting of π-type bands

It is interesting that the bandgap of germanene nanomesh (P,Q) can be opened by the hexagonal antidot only when $Q = 3m$. So, an interesting question could be raised: would the opened bandgap be immediately switched off providing the Dirac cone to be slightly shifted away from Γ point? Considering in the fact that some perturbations such as the uniaxial strain could indeed disturb the position of the Dirac cone, this issue would be fundamentally important, which may challenge the application of such germanene nanomesh as field-effect transistors to maintain the opened bandgap. Here, we would like firstly to illustrate the effects of uniaxial strain by studying the $(1,1)$ PGS. In the free-standing $(1,1)$ PGS, the Dirac cone is located at $\eta\boldsymbol{\Gamma}_1\boldsymbol{Y}_1$ with $\eta = 2/3$. In Fig. 3, the effects of the uniaxial strain are presented. By applying uniaxial strain σ_a along the armchair direction $\boldsymbol{A}_1$, the Dirac cone could be moved toward Y_1 ($\eta > 2/3$). While, the uniaxial strain σ_z applied along the zigzag direction $\boldsymbol{B}_1$ would move it toward Γ ($\eta < 2/3$). Besides the Dirac point move, the physical properties would also bear some effects of the uniaxial strain loading.

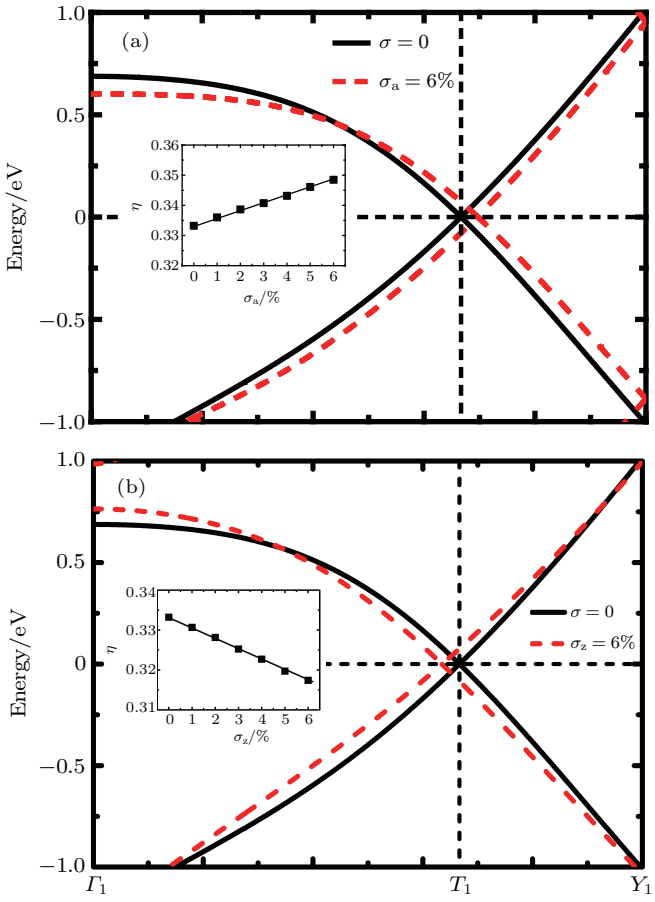


Fig. 3. (color online) The shifts of Dirac point along ΓY for the germanene under 6% uniaxial strain applied along armchair (a) and zigzag (b) edges, respectively. The insets show the deviation of Dirac point referred to its position in the free-standing germanene as a function of the applied strain. Only the bands those cross to form Dirac point are shown for clarity. The notations of k-points Γ_1, T_1, and Y_1 are illustrated in Fig. 2(b).

As for the $(1,1)$ PGS studied in Fig. 3, the 6% σ_a (σ_z) would slightly increase (decrease) the group velocities of charge carriers. The change of the group velocities is only about 1%. As for the $Q = 3m$ type PGS (P,Q), we use the $(3,3)$ as a prototype to discuss the Dirac point moving and the band splitting. Figures 4(a) and 4(b) show the presence of Dirac cone at Γ point of the free-standing $(3,3)$ PGS. By applying the strain σ_z of 4%, the studied bandstructure along the $Y'\Gamma Y$ path has been shown in Fig. 4(c). Obviously, two Dirac cones formed around Γ points. Two opposite Dirac cones, which have contrary chirality characters in the spirit of the pseudo-spin concept, are now shifted away from Γ point along opposite directions. Similar effects have also been obtained in our studies by applying σ_a strain. Therefore, we would like to concentrate on discussing the effects of σ_z strain hereafter, whose conclusions could shed light on the effects of the σ_a strain.

Compared with the bandstructure of the free-standing $(3,3)$ PGS shown in Fig. 4(a), two crossing points at Γ point now appear above and below Fermi level respectively marked as π_a and π_z in the corresponding bandstructure calculated for the strained lattice in Fig. 4(c). With the purpose to understand the physics of the Dirac cone move induced by the strain, we have studied the band decomposed charge densities of bands π_a and π_z in Figs. 4(e) and 4(f), which obviously correspond to the bonds along armchair edge and zigzag edge, respectively. Therefore, we would like to respectively refer them as the π_a and π_z bonds to facilitate the discussion hereafter. In the free-standing $(3,3)$ PGS, all the Ge–Ge bonds are almost the same with the length of about 2.44 Å. After applying the $\sigma_z = 4\%$ strain, the π_z bonds are elongated of about 2% while the π_a ones are only slightly contracted. In the spirit of the tight-binding method[42] which is believed to be effective in dealing with the π-type bands of sheet materials, the longer the bonds are, the smaller the transfer integrals are. The different changes of Ge–Ge bonds along armchair and zigzag edges result in different transfer integrals, which in turn split the degenerate π-like bands into π_a and π_z bands. The crossings of the split π bands at Fermi level form the Dirac cones around Γ. Therefore, the energy interval between π_a and π_z bands at Γ point could be used to measure the strain strength to some sense, which would be referred as E_{strain} hereafter. Due to the decrease of the vertical displacement between the buckled layers of germanene, the strain also makes an empty conducting band in Fig. 4(c) to lower down, which could be seen by comparing the bandstructures shown in Figs. 4(a) and 4(c). Actually, we have studied also the band decomposed charge density of this band, which suggests the σ-like covalent bond characters. In our studies, we found that the lowering of this σ band can be realized by applying either uniaxial or equi-biaxial strains, while the band splitting of π bands would not happen under the conditions of applying equi-biaxial strain.

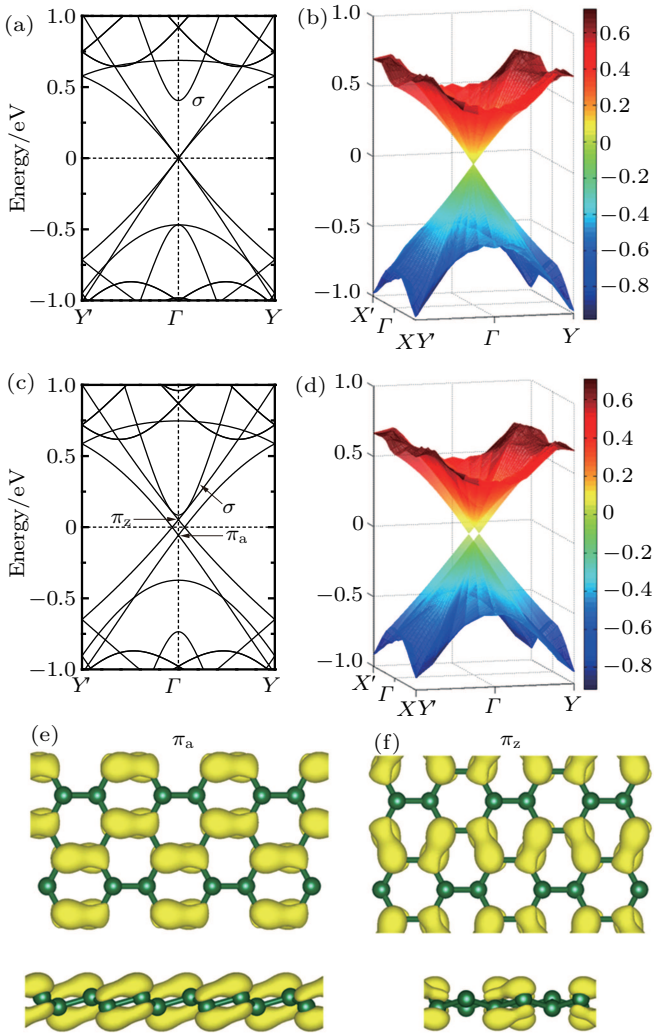


Fig. 4. (color online) The band structure along Y'–Γ–Y path (a) and the three-dimensional plotting of the corresponding Dirac cone (b) for the free-standing $(3,3)$ PGS. Those for the $(3,3)$ PGS under 4% σ_z strain are shown in panels (c) and (d), respectively. The band-decomposed charge densities at isovalue of ~ 0.01 e/Å^3 for the split π_a and π_z bands are presented in panels (e) and (f), respectively. Both top and side views are shown.

3.3. Reversible bandgap opening/closing

Now, we start to discuss the question whether the bandgap could still keep opened in the (P,Q) $(Q = 3m)$ nanomesh providing the Dirac cone to be slightly shifted away from Γ point. For the $(3,3)$ PGS with Dirac cone at Γ point, we can introduce an inversion symmetry preserved D_{6h} defect into its repeated unit cell to pattern the superlattice. As shown in Fig. 5(a), the Ge–Ge bonds of the highlighted germanium hexagon are contracted of about 3.5% to enhance their transfer integrals to mimic a D_{6h} defect. In our bandstructure studies, a sizable bandgap is opened due to the new bandgap opening mechanism. After introducing the D_{6h} defect in the repeated unit of the 4% σ_z strain engineered $(3,3)$ PGS, we have fond that this defect in fact does not change its semimetal conducting nature, though it however still splits the π_a (π_z) into

π_{a1} and π_{a2} (π_{z1} and π_{z2}) bands with energy interval E_{defect}. The crossings of π_{a2} and π_{z2} bands at the Fermi level account for the presence of two Dirac cones around Γ, realizing the bandgap closing by applying unixial strain in comparison with the free-standing D_{6h}-defect patterned $(3,3)$ nanomesh. In order to understand the physical properties of the split bands, we have studied their band decomposed charge densities, which are shown in Fig. 5(c). It is clearly shown that the π_a bands are now divided into two groups, which we would like to discuss as π_{a1} and π_{a2} bonds. We have measured the corresponding bond length changes. Under the σ_z strain of 4%, the π_a bonds in the defect-free PGS (the one studied in Fig. 4(c)) are almost the same in length. After introducing the defect in the unit cell, the π_{a1} bonds are contracted of $\sim 0.6\%$ while the π_{a2} bonds are elongated of $\sim 0.4\%$, resulting in the different transfer integrals accordingly to inducing the splitting of π_a bands. Similarly, the π_{z1} bonds are elongated of $\sim$0.5% while the π_{z2} bonds are contracted of $\sim$0.3%, accounting for the splitting of π_z bands.

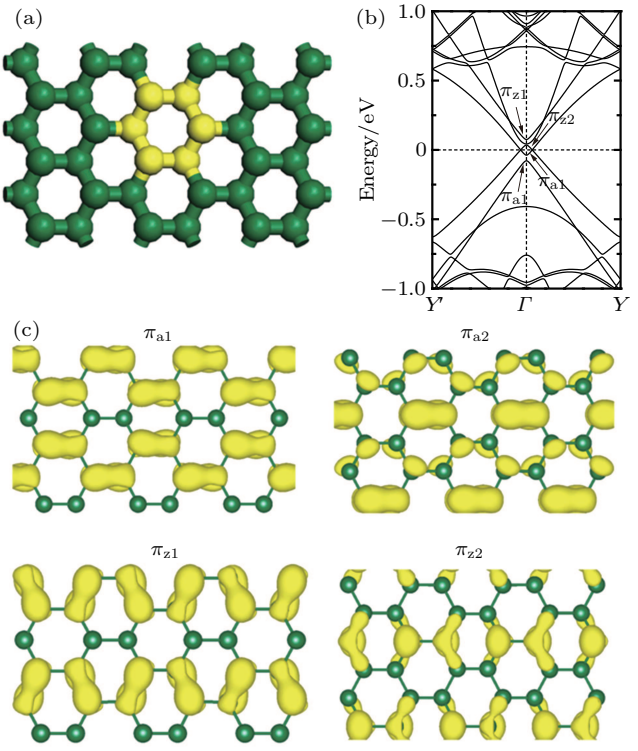


Fig. 5. (color online) The D_{6h} defect formed by contracting the Ge–Ge bonds by 3.5% of the grey (yellow online) hexagon (a) and the corresponding band structure along the Y'–Γ–Y path (b). The corresponding band-decomposed charge densities at isovalue of ~ 0.01 e/Å^3 for the split π_{a1}, π_{a2}, π_{z1}, and π_{z2} bands are shown in panel (c).

Based on our detailed studies, the bandgap opening/closing could in fact be determined by the competition between the energy split intervals E_{defect} induce by the defect and the E_{strain} attributed to the uniaxial strain. In the defect patterned $(3,3)$ superlattice presented in Fig. 5(b), E_{defect} and E_{strain} are respectively 0.04 eV and 0.12 eV, where the bandgap is closed due to the fact of $E_{defect} < E_{strain}$. As for the free-standing one, the E_{strain} equals to zero while the E_{defect} is still of ~ 0.04 eV, where a bandgap is opened ($E_{defect} > E_{strain}$). With the purpose to shed light on the experimental studies of vacancy hole patterned nanomesh, we have also studied the phenomena of bandgap opening/closing in antidot patterned germanium nanomesh. The results of the Ge_6 antidot patterned $(6,6)$ nanomesh are presented in Fig. 6. For the defect free $(6,6)$ PGS, the Dirac cone is found at Γ point when $\sigma_z = 0\%$. Enhancing the strain, the Dirac cone formed by π band crossing at Fermi level could be moved away from Γ. The band of the empty σ covalent bond would be lowered downward also by the strain, which even dip below the Fermi level for the case under $\sigma_z = 6\%$ strain. After introducing the Ge_6 antidot in unit cell, the free-standing $(6,6)$ nanomesh opens a sizable bandgap of about 0.13 eV, which stands for the E_{defect}. Applying uniaxial strain, the E_{strain} starts to increase, while the E_{defect} only changes slightly. Under $\sigma_z = 3\%$, due to the fact of $E_{defect} > E_{strain}$, the bandgap keeps opened while its width is reduced to ~ 0.06 eV. After enhancing strain to $\sigma_z = 6\%$, the situation changes and the π_{a2} and π_{z2} start to

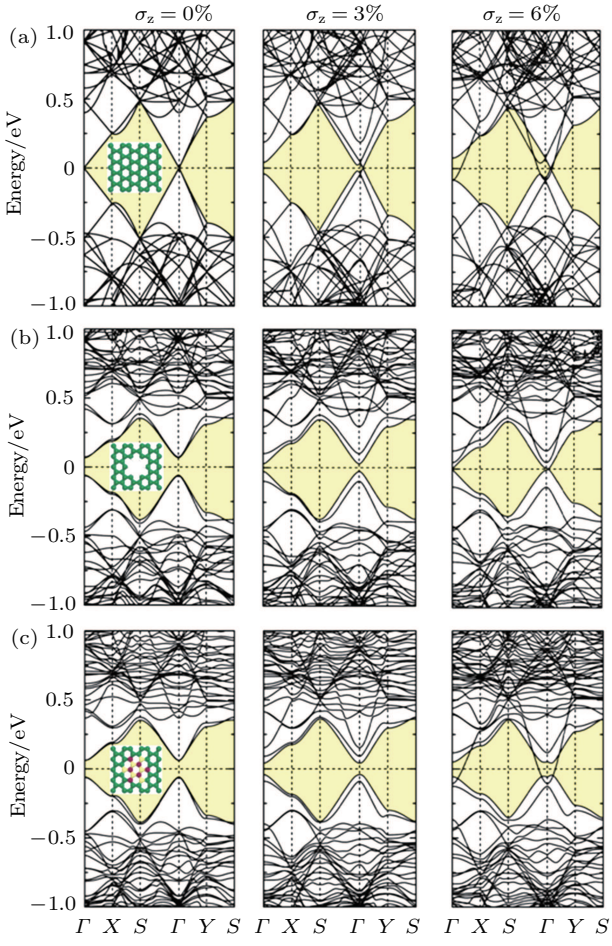


Fig. 6. (color online) The calculated band structures for the germanene-based nanostructures under the 3% and 6% σ_z strains and the ones for the free-standing materials. The panels (a), (b), and (c) are for the $(6,6)$ PGS, Ge_6-patterned nanomesh, and $(GaAs)_6$-patterned superlattice, respectively.

cross to form new Dirac cone. The high velocity massless fermions as charge carriers would present again, suggesting a reversible on/off switch of bandgap. Probably due to the presence of Ge_6 antidot, the local strain is released to some sense, which may account for the increase of the σ band as referred to the case of its counterpart — the defect free $(6,6)$ PGS. In comparison, by substitution doping a $(GaAs)_6$ nanoflake in the unit cell, the local strain would probably preserved due to the well match between the lattice constants of Ge and GaAs diamond bulk structures. As shown in Fig. 6(c), it could keep the σ band to dip below Fermi level for the case under $\sigma_z = 6\%$ strain. Carefully analyzing the band structures of the antidot-patterned $(6,6)$ nanomesh and the $(GaAs)_6$ patch-patterned superlattice, one can see that the gap between the π-type bands around Fermi level show quite different characters. In the former one, the uniaxial strain can engineer the gap width, even to close it when the π_{a2} and π_{z2} start to cross. However, in the latter case, the π-band gap width keeps almost unchanged in the process of applying strain. This confirms again the different mechanisms in opening their bandgaps. The π-band gap opened through breaking the sublattice equivalence in the $(GaAs)_6$ patch-patterned superlattice cannot be engineered by manipulating strain. As shown in Fig. 6(c), the conducting properties of $(GaAs)_6$ patch-patterned superlattice could in fact also be altered from semiconductor to conductor due to the σ band dipped below the Fermi level.

4. Conclusions

To summarize, we have carried out detailed studies of the combination effects of the uniaxial strain and the degenerate perturbation on the electronic structure engineering of germanene nanomesh. Both uniaxial strains applied along armchair and zigzag edges could move Dirac point along $\boldsymbol{\Gamma Y}$ path in Brilliouin zone, making the degenerate π-like bands to split into π_a and π_z bands with energy interval E_{strain}. For the free-standing (P,Q) PGS with $Q = 3m$ (m is integer), the Dirac cone would be folded to Γ point according to band-folding analysis, which could be then opened a bandgap by introducing in the inversion symmetry preserved defect. The bandgap opening can be attributed to the band splitting of π_a (π_z) into π_{a1} and π_{a2} bands (π_{z1} and π_{z2} bands) with split interval E_{defect}, showing different bandgap opening mechanism in comparison with the one by breaking sublattice equivalence. For a nanomesh, the E_{defect} of the π-band splitting only changes slightly while the E_{strain} could be enlarged by enhancing the uniaxial strain. Then, the bandgap could be controlled to open or close by the competition between E_{defect} and E_{strain}. Before band closing, its width could also be continuously tuned through controlling strain. The nanomesh patterned with $(GaAs)_6$ nanoflake patches has also been studied, whose bandgap has been opened by the sublattice equivalence breaking. Here, the π-band split gap remains almost unaffected by the applied strain.

Acknowledgment

We thank Dr. J Guo and Dr. J Liu for carefully reading through our manuscript.

References

[1] Novoselov K S, Geim A K, Mozorov S V, Jiang D, Zhang Y, Dubonos S V, Grigorieva I V and Firsov A A 2004 *Science* **306** 666
[2] Novoselov K S, Geim A K, Morozov S V, Jiang D, Katsnelson M I, Grigorieva I V, Dubonos S V and Firsov A A 2005 *Nature* **438** 197
[3] Zhang Y, Tan Y-W, Stormer H L and Kim P 2005 *Nature* **438** 201
[4] Wang J, Duan X M and Zhang P 2016 *Chin. Phys. B* **25** 057301
[5] Yang, Y, Cao J X and Yang W 2008 *Chin. Phys. B* **17** 1881
[6] Guo Y H, Cao J X and Xu B 2016 *Chin. Phys. B* **25** 017101
[7] Wu X G 2016 *Chin. Phys. B* **25** 117801
[8] Wei Y, Jia T and Chen G 2017 *Chin. Phys. B* **26** 028103
[9] Lin C L, Arafune R, Kawai M and Takagi N 2015 *Chin. Phys. B* **24** 87307
[10] Li H, Fu H X and Meng S 2015 *Chin. Phys. B* **24** 086102
[11] Wang H B, Su Y and Chen G 2014 *Chin. Phys. B* **23** 018103
[12] Tang Q and Zhou Z 2013 *Prog. Mater. Sci.* **58** 1244
[13] Meng L, Wang Y, Zhang L, Du S, Wu R, Li L, Zhang Y, Li G, Zhou H, Hofer W A and Gao H J 2013 *Nano Lett.* **13** 685
[14] Zhao T, Zhang S, Wang Q, Kawazoe Y and Jena P 2014 *Phys. Chem. Chem. Phys.* **16** 22979
[15] Padiha J E and Pontes R B 2016 *Solid State Commun.* **225** 38
[16] Guzmán-Verri G G and Lew Yan Voon L C 2007 *Phys. Rev. B* **76** 075131
[17] Nijamudheen A, Bhattacharjee R, Choudhury S and Datta A 2015 *J. Phys. Chem. C* **119** 3802
[18] Oughaddou H, Sawaya S, Goniakowski J, Aufray B, Le Lay G, Gay J M, Tréglia G, Bibérian J P, Barrett N, Guillot C, Mayne A and Dujardin G 2000 *Phys. Rev. B* **62** 16653
[19] Li L, Lu S, Pan J, Qin Z, Wang Y, Wang Y, Cao G, Du S and Gao H 2014 *Adv. Mater.* **26** 4820
[20] Dávila M E, Xian L, Cahangirov S, Rubio A and Le Lay G 2014 *New J. Phys.* **16** 095002
[21] Derivaz M, Dentel D, Stephan R, Hanf M-C, Mehdaoui A, Sonnet P and Pirri C 2015 *Nano Lett.* **15** 2510
[22] Yuan J, Tang C, Zhong J and Mao Y 2015 *Appl. Surf. Sci.* **360** 707
[23] Matthes L, Pulci O and Bechstedt F 2014 *New J. Phys.* **16** 105007
[24] Deng Z, Li Z and Wang W 2015 *Chem. Phys. Lett.* **637** 26
[25] Kaloni T P, Modarresi M, Tahir M, Roknabadi M R, Schreckenbach G and Freund M 2015 *J. Phys. Chem. C* **119** 11896
[26] Li Y and Chen Z 2014 *J. Phys. Chem. C* **118** 1148
[27] Xiao P, Fan X L and Liu L M 2014 *Comp. Mater. Sci.* **92** 244
[28] Wang X Q, Li H D and Wang J T 2012 *Phys. Chem. Chem. Phys.* **14** 3031
[29] Pang Q, Zhang C L, Li L, Fu Z Q, Wei X M and Song Y L 2014 *Appl. Surf. Sci.* **314** 15
[30] Pang Q, Li L, Zhang C L, Wei X M and Song Y L 2015 *Mater. Chem. Phys.* **160** 96
[31] Kaloni T P 2014 *J. Phys. Chem. C* **118** 25200
[32] Li S J, Su Y and Chen G 2015 *Chem. Phys. Lett.* **638** 187
[33] Meng Y, Quhe R, Zheng J, Ni Z, Wang Y, Yuan Y, Tse G, Shi J, Gao Z and Lu J 2014 *Physica E: Low-dimens. Syst. Nanostruct.* **59** 60
[34] Broek B, Houssa M, Scalise E, Pourtois G, Afanas'ev V V and Stesmans A 2014 *Appl. Surf. Sci.* **291** 104
[35] Gong L, Xiu S L, Zheng M M, Zhao P, Zhang Z, Liang Y Y, Chen G and Kawazoe Y 2014 *J. Mater. Chem. C* **2** 8773
[36] Kresse G and Furthmüller J 1996 *Phys. Rev. B* **54** 11169
[37] Kresse G and Joubert D 1999 *Phys. Rev. B* **59** 1758
[38] Perdew J P, Burke K and Ernzerhof M 1996 *Phys. Rev. Lett.* **77** 3865
[39] Monkhorst H J and Pack J D 1976 *Phys. Rev. B* **13** 5188
[40] Yang J, Ma M, Li L, Zhang Y, Huang W and Dong X 2014 *Nanoscale* **6** 13301
[41] Xiu S L, Zheng M M, Zhao P, Zhang Y, Liu H Y, Li S J, Chen G and Kawazoe Y 2014 *Carbon* **79** 646
[42] Singleton J 2001 *Band Theory and Electronic Properties of Solids* (New York: Oxford University Press)